# Photoionization, Recombination, and Radiative Transitions of Atoms and Ions

Sultana N. Nahar
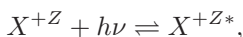
Department of Astronomy, The Ohio State University, Columbus, OH 43210, USA
`nahar@astronomy.ohio-state.edu`

**Summary.** Physical properties such as temperature, density of stars and their chemical compositions can be obtained from detail analysis of their spectra at various wavelengths. Ultraviolet (UV) wavelengths are particularly important as the chromosphere surrounding a star is rich in UV radiation generated by collisional and radiative atomic processes, such as photoionization, electron-ion recombination and bound-bound radiative transitions in the plasma. For both precise diagnostics and astrophysical modelings, accurate atomic parameters for these processes are essential. I report the latest developments in theoretical quantum mechanical calculations, especially under the two international collaborations known as the Opacity Project (OP, The Opacity Project Team 1995, 1996) and the Iron Project (IP, series in A&A 1993-), that have yielded accurate and large-scale atomic data for photoionization cross sections, oscillator strengths, and collision strengths for electron impact excitation of the most astrophysically abundant atoms and ions, and the extension, total and level-specific electron-ion recombination cross sections and rates. The calculations are carried out in an *ab initio* manner using the accurate and powerful R-matrix method, including relativistic fine structure effects for many ions, in the close-coupling approximation.

## 1 Radiative Atomic Processes

There are three dominant atomic radiative processes in astrophysical plasmas. (1) Bound-bound transition - radiative excitation and de-excitation:

$$X^{+Z} + h\nu \rightleftharpoons X^{+Z*},$$

where $X^{+Z}$ is the ion with charge $Z$. The emitted or absorbed photon ($h\nu$) is observed as a spectral line. The relevant atomic parameters for the direct and inverse processes are oscillator strength ($f$) and radiative decay rate ($A$-value). Astrophysical opacities depend largely on the $f$-values of all transitions.

The other two are the inverse processes of (2) photoionization (PI) and (3) electron-ion recombination. These two proceed in two ways: (i) direct photoionization and radiative recombination (RR):

$$X^{+Z} + h\nu \rightleftharpoons X^{+Z+1} + \epsilon,$$

(ii) photoionization with autoionization (AI) and dielectronic recombination (DR):

$$e + X^{+Z} \rightleftharpoons (X^{+Z-1})^{**} \rightleftharpoons \begin{cases} e + X^{+Z}. & \text{(AI)} \\ X^{+Z-1} + h\nu. & \text{(DR)} \end{cases}$$

*The intermediate doubly excited "autoionizing state" introduces resonances in the process.* Photoionization resonances can be seen in absorption spectra while recombination resonances can be seen in emission spectra. The atomic parameters for processes (2) and (3) are photoionization cross sections ($\sigma_{PI}$), recombination cross sections ($\sigma_{RC}$) and rate coefficients ($\alpha_{RC}$). These quantities determine, for example, ionization fractions in astrophysical plasmas.

## 2 Theory

The Schrödinger equation for an (N+1)-electron system in nonrelativistic LS coupling is

$$H_{N+1}^{NR}\Psi = \left[\sum_{i=1}^{N+1}\left\{-\nabla_i^2 - \frac{2Z}{r_i} + \sum_{j>i}^{N+1}\frac{2}{r_{ij}}\right\}\right]\Psi = E\Psi. \tag{1}$$

Relativistic effects can be included as perturbation via three one-body correction terms in the Hamiltonian:

$$H_{N+1}^{\mathrm{BP}} = H_{N+1}^{NR} + H_{N+1}^{\mathrm{mass}} + H_{N+1}^{\mathrm{Dar}} + H_{N+1}^{\mathrm{so}}, \tag{2}$$

where $H^{mass} = -\frac{\alpha^2}{4}\sum_i p_i^4$, $H^{Dar} = \frac{\alpha^2}{4}\sum_i \nabla^2\left(\frac{Z}{r_i}\right)$, $H^{so} = \left[\frac{Ze^2\hbar^2}{2m^2c^2r^3}\right]\mathbf{L.S.}$

These are implemented in the R-matrix method, under the IP, with the name the Breit-Pauli R-matrix (BPRM) method. The spin-orbit interaction $H^{so}$ splits LS energy into fine structure levels. However, the energies can be further improved with additional higher order correction terms, such as the Breit interaction term, the spin-spin interaction term, etc. (e.g. Nahar et al. 2003).

The close coupling (CC) approximation for the wavefunction treats an atomic system as of (N+1) electrons: the target or the core ion of N electrons and the interacting (N+1)th electron (e.g. Seaton 1987). The total wavefunction expansion is expressed as:

$$\Psi_E(e + ion) = A\sum_i^N \chi_i(ion)\theta_i + \sum_j c_j\Phi_j(e + ion),$$

where $\chi_i$ is the target ion or core wavefunction at state $i$, $\theta_i$ is the interacting electron wavefunction, which can be in continuum or bound depending on its energy, and $\Phi_j$ is a correlation function of (e+ion). Substitution of $\Psi_E(e + ion)$ in the Hamiltonian equation results in a set of coupled equations which are solved by the R-matrix method. The solution $\Psi_B$ is of a bound state when E < 0 or $\Psi_F$ of a continuum state when E ≥ 0. The complex resonant

structures in the atomic processes are introduced through couplings of bound and continuum channels in the transition matrix.

For radiative processes, the transition matrix elements $< \Psi_B||\mathbf{D}||\Psi_{B'} >$ are for bound-bound transitions and $< \Psi_B||\mathbf{D}||\Psi_F >$ for photoionization and recombination. $\mathbf{D} = \sum_i \mathbf{r}_i$ is the dipole operator of $i$ electrons. The quantity of interest $S$, the generalized line strength, can be obtained as

$$S = \left| \left\langle \Psi_f| \sum_{j=1}^{N+1} r_j |\Psi_i \right\rangle \right|^2. \tag{3}$$

The oscillator strength ($f_{ij}$) and the radiative decay rate ($A_{ji}$) for a dipole bound-bound transition are

$$f_{ij} = \left[ \frac{E_{ji}}{3g_i} \right] S, \quad A_{ji}(sec^{-1}) = \left[ 0.8032 \times 10^{10} \frac{E_{ji}^3}{3g_j} \right] S. \tag{4}$$

The photoionization cross section, $\sigma_{PI}$, is related to $S$ as

$$\sigma_{PI} = \left[ \frac{4\pi}{3c} \frac{1}{g_i} \right] \omega S, \tag{5}$$

where $\omega$ is the incident photon energy in Rydberg units.

The recombination cross section, $\sigma_{RC}$, can be obtained from $\sigma_{PI}$ using the principle of detailed balance (Milne relation) as

$$\sigma_{RC} = \sigma_{PI} \frac{g_i}{g_j} \frac{h^2\omega^2}{4\pi^2 m^2 c^2 v^2}. \tag{6}$$

The recombination rate coefficient, $\alpha_{RC}$, is obtained as

$$\alpha_{RC}(T) = \int_0^\infty v f(v) \sigma_{RC} dv, \tag{7}$$

where $f(v,T) = \frac{4}{\sqrt{\pi}} (\frac{m}{2kT})^{3/2} v^2 e^{-\frac{mv^2}{2kT}}$ is the Maxwellian velocity distribution function. The total $\alpha_{RC}$ is obtained from summed contributions of an infinite number of recombined states.

The unified theory for electron-ion recombination considers all infinite recombining levels and subsumes RR and DR in a unified manner (Nahar & Pradhan 1992, 1994; Zhang et al. 1999). Existing methods treat RR and DR separately and the total rate is obtained from $\alpha_{RC} = \alpha_{RR} + \alpha_{DR}$, neglecting the interference between RR and DR. The unified method divides the recombined states into two groups. The contributions from states with $n \leq 10$ (group A) are obtained from $\sigma_{PI}$ using the principle of detailed balance, while the contributions from states with $10 < n \leq \infty$ (group B), which are dominated by narrow dense resonances, are obtained from an extension of the DR theory (Bell & Seaton 1985; Nahar & Pradhan 1994). The method

provides a self-consistent set of $\sigma_{PI}$, $\sigma_{RC}$, and $\alpha_{RC}$ as they are obtained using the same wavefunction. It also provides level-specific recombination rate coefficients and photoionization cross sections for many bound levels.

An application of the self-consistent results is the determination of the ionization fractions in plasma equilibria. At coronal equilibrium, the electron impact ionization is balanced by the electron-ion recombination

$$N(z-1)S(z-1) = N(z)\alpha_{RC}(z), \tag{8}$$

where $S(z-1)$ is the total electron impact ionization rate coefficient and $\alpha_{RC}$ is the total (RR+DR) recombination rate coefficient. Photoionization equilibrium in the presence of a radiative source is maintained by the balance of photoionization and electron-ion recombination

$$N(z)\int_{\nu_0}^{\infty}\frac{4\pi J_\nu}{h\nu}\sigma_{PI}(z,\nu)d\nu = N_e N(z+1)\alpha_{RC}(z,T_e), \tag{9}$$

where $J_\nu$ is photoionizing radiation flux, $\nu_0$ is ionization potential of the ion, and $\sigma_{PI}$ is photoionization cross section. Use of self-consistent data for $\sigma_{PI}$ on the left-hand-side, and $\alpha_{RC}$ on the right-hand-side, will provide accurate ionization fractions.

## 3 Results

Results with features on oscillator strengths and radiative decay rates for bound-bound transitions, photoionization cross sections and recombination rate coefficients are illustrated below. An update on data accessibility for the latest monochromatic opacities is given in the last subsection.

### 3.1 Radiative Transitions - $f$, $S$, $A$-values

Under the IP, $f$, $S$, and $A$-values for fine structure transitions in all ionization stages of iron and other astrophysically abundant atoms and ions are being calculated. Both the allowed and forbidden transitions are considered as summarized below.

Allowed electric dipole (E1) transitions are of two types: (i) dipole allowed ($\Delta j=0,\pm1$, $\Delta L = 0, \pm1, \pm2$, $\Delta S = 0$, parity $\pi$ changes), (ii) intercombination ($\Delta j=0,\pm1$, $\Delta L = 0, \pm1, \pm2$, $\Delta S \neq 0$, $\pi$ changes):

$$A_{ji}(sec^{-1}) = 0.8032 \times 10^{10}\frac{E_{ji}^3}{3g_j}S^{E1}, \quad f_{ij} = \frac{E_{ji}}{3g_i}S^{E1}(ij), \tag{10}$$

where $S^{E1}(ij)$ is the line strength for E1 transition.

Forbidden transitions, which are usually much weaker than the allowed transitions, are of higher order magnetic and electric poles.
i) Electric quadrupole (E2) transitions ($\Delta J = 0,\pm1,\pm2$, parity does not change):

$$A_{ji}^{E2} = 2.6733 \times 10^3\frac{E_{ij}^5}{g_j}S^{E2}(i,j) \text{ s}^{-1}, \tag{11}$$

ii) Magnetic dipole (M1) transitions ($\Delta J = 0, \pm 1$, parity does not change):

$$A_{ji}^{M1} = 3.5644 \times 10^4 \frac{E_{ij}^3}{g_j} S^{M1}(i,j) \text{ s}^{-1}, \tag{12}$$

iii) Electric octupole (E3) transitions ($\Delta J = \pm 2, \pm 3$, parity changes):

$$A_{ji}^{E3} = 1.2050 \times 10^{-3} \frac{E_{ij}^7}{g_j} S^{E3}(i,j) \text{ s}^{-1}, \tag{13}$$

iv) Magnetic quadrupole (M2) transitions ($\Delta J = \pm 2$, parity changes):

$$A_{ji}^{M2} = 2.3727 \times 10^{-2} \text{s}^{-1} \frac{E_{ij}^5}{g_j} S^{M2}(i,j). \tag{14}$$

The lifetime of a level can be calculated from the $A$-values:

$$\tau_k(s) = 1/\sum_i A_{ki}(s^{-1}). \tag{15}$$

E1 transitions are considered for levels going up to $n=10$ and $l \leq 9$ while weaker forbidden transitions are typically up to $n \leq 5$. All calculated BPRM energy levels are identified spectroscopically using a theoretical quantum defect procedure (Nahar & Pradhan 2000) and are shown in Table 1 as an example (Nahar et al. 2007). Examples of allowed and forbidden transitions are presented in Tables 2 and 3 respectively. Transitions of many ions are available from the author and from CDS (series in A&A 1993-); a partial list includes: Fe V, Fe XVII, Fe XVIII, Fe XXI, Fe XXIII, Fe XXIV, Fe XXV, C IV, N V, O VI, F VII, Ne VIII, Na IX, Mg X, Al XI, Si XII, S XIV, Ar XVI, Ca XVIII, Ti XX, Cr XXII, Ni XXVI, C IV, N V, O VI, F VII, Ne VIII, Na IX, Mg X, Al XI, Si XII, S XIV, Ar XVI, Ca XVIII, Ti XX, Cr XXII, Ni XXVI, C II, C III, O IV, S II, Ar XIII, Na III, Cl-like ions

## 3.2 Photoionization - Cross Sections and Resonances

Under the OP and IP, the photoionization cross sections $\sigma_{PI}$ are obtained for the ground and large number of excited bound states, typically with $n \leq 10$ and $l \leq 9$. CC approximation enables extensive resonances in $\sigma_{PI}$. Central field approximation can not generate the resonances. However, resonances exist in all atomic systems with more than one electron as examplified in Fig. 1 for H and He ground level $\sigma_{PI}$ (Nahar 2007a).

With a more complex system, such as for carbon like argon, Ar XIII, photoionization of the excited $2s2p^2\ 4P3s(^5P)$ state is dominated by high resonances which also enhance the background (Nahar 2004) as shown in Fig. 2. These structures will provide considerable contributions to quantities such as photoionization rates, recombination rates, etc., especially at high

**Table 1.** Fine structure energy levels of Fe XVI with spectroscopic identification from relativistic BPRM calculations. The last column is the code representation of the level.

| $96$ = number of levels, $n \leq 10$, $l \leq 9$ | | | | | | |
|---|---|---|---|---|---|---|
| $i_e$ | J | $i_J$ | E(Ry) | Config | $^{2S+1}L^{\pi}$ | 2jpiiii |
| 1 0.5 e | | 1 | -3.59611E+01 | $2p63s$ | $^2Se$ | 100001 |
| 2 0.5 e | | 2 | -1.89410E+01 | $2p64s$ | $^2Se$ | 100002 |
| 3 0.5 e | | 3 | -1.17032E+01 | $2p65s$ | $^2Se$ | 100003 |
| 4 0.5 e | | 4 | -7.93052E+00 | $2p66s$ | $^2Se$ | 100004 |
| 5 0.5 e | | 5 | -5.67969E+00 | $2p67s$ | $^2Se$ | 100005 |
| 6 0.5 e | | 6 | -4.33725E+00 | $2p61Se8s$ | $^2Se$ | 100006 |
| 7 0.5 e | | 7 | -3.39566E+00 | $2p61Se9s$ | $^2Se$ | 100007 |
| 8 0.5 e | | 8 | -2.73047E+00 | $2p61Se10s$ | $^2Se$ | 100008 |
| 9 0.5 o | | 1 | -3.34351E+01 | $2p63p$ | $^2Po$ | 110001 |
| 10 0.5 o | | 2 | -1.79394E+01 | $2p64p$ | $^2Po$ | 110002 |
| 11 0.5 o | | 3 | -1.12004E+01 | $2p65p$ | $^2Po$ | 110003 |
| 12 0.5 o | | 4 | -7.65350E+00 | $2p66p$ | $^2Po$ | 110004 |
| 13 0.5 o | | 5 | -5.55871E+00 | $2p61Se7p$ | $^2Po$ | 110005 |
| 14 0.5 o | | 6 | -4.22249E+00 | $2p61Se8p$ | $^2Po$ | 110006 |
| 15 0.5 o | | 7 | -3.31599E+00 | $2p61Se9p$ | $^2Po$ | 110007 |
| 16 0.5 o | | 8 | -2.67295E+00 | $2p61Se10p$ | $^2Po$ | 110008 |
| 17 1.5 e | | 1 | -2.98055E+01 | $2p63d$ | $^2De$ | 300001 |
| 18 1.5 e | | 2 | -1.65992E+01 | $2p64d$ | $^2De$ | 300002 |
| 19 1.5 e | | 3 | -1.05545E+01 | $2p65d$ | $^2De$ | 300003 |
| 20 1.5 e | | 4 | -7.29200E+00 | $2p66d$ | $^2De$ | 300004 |

.......

**Table 2.** Example set of $f$-, $S$, and $A$ values for E1 (dipole allowed and intercombination) transitions in Fe XVI with n $\leq$ 10, l $\leq$ 9.

| Ion: Z=26 | | Ne=11 | | | | | | | | |
|---|---|---|---|---|---|---|---|---|---|---|
| $I_i$ | $I_k$ | $\lambda(\mathring{A})$ | $E_i$(Ry) | $E_k$(Ry) | | $f$ | | $S$ | | $A_{ki}(s^{-1})$ |
| | 2 | 0 | 2 | 1 8 8 | 64= | gi Pi | gk Pk | Ni Nk | NN | |
| 1 | 1 | 360.75 | -3.5961E+01 | -3.3435E+01 | | -1.210E-01 | | 2.873E-01 | | 6.199E+09 |
| 1 | 2 | 50.56 | -3.5961E+01 | -1.7939E+01 | | -7.854E-02 | | 2.615E-02 | | 2.049E+11 |
| 1 | 3 | 36.80 | -3.5961E+01 | -1.1200E+01 | | -2.276E-02 | | 5.516E-03 | | 1.121E+11 |
| 1 | 4 | 32.19 | -3.5961E+01 | -7.6535E+00 | | -1.173E-02 | | 2.486E-03 | | 7.549E+10 |
| 1 | 5 | 29.97 | -3.5961E+01 | -5.5587E+00 | | -6.351E-03 | | 1.253E-03 | | 4.716E+10 |
| 1 | 6 | 28.71 | -3.5961E+01 | -4.2225E+00 | | -3.817E-03 | | 7.216E-04 | | 3.088E+10 |
| 1 | 7 | 27.91 | -3.5961E+01 | -3.3160E+00 | | -2.487E-03 | | 4.572E-04 | | 2.129E+10 |
| 1 | 8 | 27.38 | -3.5961E+01 | -2.6730E+00 | | -1.720E-03 | | 3.100E-04 | | 1.531E+10 |
| 2 | 1 | 62.87 | -1.8941E+01 | -3.3435E+01 | | 6.452E-02 | | 2.671E-02 | | 1.089E+11 |
| 2 | 2 | 909.81 | -1.8941E+01 | -1.7939E+01 | | -1.790E-01 | | 1.072E+00 | | 1.442E+09 |
| 2 | 3 | 117.73 | -1.8941E+01 | -1.1200E+01 | | -7.449E-02 | | 5.774E-02 | | 3.584E+10 |
| 2 | 4 | 80.73 | -1.8941E+01 | -7.6535E+00 | | -3.257E-02 | | 1.732E-02 | | 3.334E+10 |
| 2 | 5 | 68.10 | -1.8941E+01 | -5.5587E+00 | | -1.445E-02 | | 6.476E-03 | | 2.078E+10 |

**Table 3.** Example set of radiative decay rates in $s^{-1}$ for the forbidden electric quadrupole (AE2), electric octupole (AE3), magnetic dipole (AM1), and magnetic quadrupole (AM2) transitions in Fe XVI (Nahar et al. 2007). $T$s denote the terms with configurations numbered as: $2p^63s(1),2p^63p(2),, 2p^63d(3), 2p^64s(4), 2p^64p(5), 2p^64d(6), 2p^64f(7), 2p^65s(8), 2p^65p(9), 2p^65d(10), 2p^65f(11), 2p^65g(12),2p^53s^2(13), 2p^53s3p(14), 2p^53s3d(15), 2p^53s4s(16), 2p^53s4p(17), 2p^53s4d(18), 2p^53s4f(19), 2p^53p^2(20), 2p^53p3d(21), 2s2p^63p^2(22)$. $N_{tr}$ is the number of transitions.

| i- j | $T_i\ C_i - T_j\ C_j$ | $g_i - g_j$ | $\lambda(\text{Å})$ | $E_i(\text{Ry})$ | $E_j(\text{Ry})$ | AE2 | AM1 |
|---|---|---|---|---|---|---|---|
| | | | E2 and M1, $N_{tr} = 20005$ | | | | |
| 2- 3 | 2Po 2- 2Po 2 | 2- 4 | 4773 | 2.53E+00 | 2.72E+00 | 2.36E-02 | 8.26E+01 |
| 1- 4 | 2Se 1- 2De 3 | 2- 4 | 148.04 | 0.00E+00 | 6.16E+00 | 6.61E+05 | 9.18E-01 |
| 1- 5 | 2Se 1- 2De 3 | 2- 6 | 147.40 | 0.00E+00 | 6.18E+00 | 6.78E+05 | 0.00E+00 |
| 4- 5 | 2De 3- 2De 3 | 4- 6 | 34387 | 6.16E+00 | 6.18E+00 | 2.49E-07 | 2.65E-01 |
| 1- 6 | 2Se 1- 2Se 4 | 2- 2 | 53.54 | 0.00E+00 | 1.70E+01 | 0.00E+00 | 7.24E+01 |
| 4- 6 | 2De 3- 2Se 4 | 4- 2 | 83.88 | 6.16E+00 | 1.70E+01 | 9.00E+06 | 1.38E-01 |
| 5- 6 | 2De 3- 2Se 4 | 6- 2 | 84.08 | 6.18E+00 | 1.70E+01 | 1.36E+07 | 0.00E+00 |
| 2- 7 | 2Po 2- 2Po 5 | 2- 2 | 58.81 | 2.53E+00 | 1.80E+01 | 0.00E+00 | 3.76E+01 |
| 3- 7 | 2Po 2- 2Po 5 | 4- 2 | 59.54 | 2.72E+00 | 1.80E+01 | 6.84E+07 | 4.83E+03 |
| 2- 8 | 2Po 2- 2Po 5 | 2- 4 | 58.53 | 2.53E+00 | 1.81E+01 | 3.42E+07 | 2.06E+03 |
| 3- 8 | 2Po 2- 2Po 5 | 4- 4 | 59.26 | 2.72E+00 | 1.81E+01 | 3.41E+07 | 1.38E+02 |
| 7- 8 | 2Po 5- 2Po 5 | 2- 4 | 12483 | 1.80E+01 | 1.81E+01 | 2.60E-03 | 4.62E+00 |
| | | | .......... | | | | |
| | | | E3 and M2, $N_{tr} = 7078$ | | | | |
| i- j | $T_i\ C_i - T_j\ C_j$ | $g_i - g_j$ | $\lambda(\text{Å})$ | $E_i(\text{Ry})$ | $E_j(\text{Ry})$ | AE3 | AM2 |
| 2- 5 | 2Po 2- 2De 3 | 2- 6 | 249.25 | 2.53E+00 | 6.18E+00 | 1.69E-01 | 3.22E+01 |
| 5- 7 | 2De 3- 2Po 5 | 6- 2 | 76.97 | 6.18E+00 | 1.80E+01 | 2.38E+03 | 2.45E+03 |
| 2- 10 | 2Po 2- 2De 6 | 2- 6 | 54.09 | 2.53E+00 | 1.94E+01 | 1.30E+04 | 1.45E+04 |
| 7- 10 | 2Po 5- 2De 6 | 2- 6 | 674.51 | 1.80E+01 | 1.94E+01 | 9.07E-03 | 9.58E-01 |
| 1- 11 | 2Se 1- 2Fo 7 | 2- 6 | 45.77 | 0.00E+00 | 1.99E+01 | 4.04E+04 | 7.29E-07 |
| 6- 11 | 2Se 4- 2Fo 7 | 2- 6 | 315.21 | 1.70E+01 | 1.99E+01 | 6.94E-01 | 3.19E-15 |
| 1- 12 | 2Se 1- 2Fo 7 | 2- 8 | 45.76 | 0.00E+00 | 1.99E+01 | 4.05E+04 | 0.00E+00 |
| 4- 12 | 2De 3- 2Fo 7 | 4- 8 | 66.23 | 6.16E+00 | 1.99E+01 | 1.93E+03 | 2.88E+04 |
| 6- 12 | 2Se 4- 2Fo 7 | 2- 8 | 314.77 | 1.70E+01 | 1.99E+01 | 7.02E-01 | 0.00E+00 |
| 9- 12 | 2De 6- 2Fo 7 | 4- 8 | 1647 | 1.94E+01 | 1.99E+01 | 5.05E-06 | 9.23E-03 |
| 11- 13 | 2Fo 7- 2Se 8 | 6- 2 | 209.63 | 1.99E+01 | 2.43E+01 | 2.18E+01 | 2.70E-15 |

temperature. The narrow resonances belong to Rydberg series, $(LS)_t\nu l$, of various target terms, $(LS)_t$, and can be determined from

$$(E_t - E_p) = z^2/\nu^2$$

where $E_t$ is the energy of the core threshold $(LS)_t$, $E_p$ is the electron energy, and $\nu$ is the effective quantum number. Resonances often overlap when the core levels are closely spaced.

The other type of resonance is the Seaton resonance (also known as the PEC, from photo-excitation-of-core) that forms at an excited core threshold (Yu & Seaton 1987; Nahar & Pradhan 1993). The core excitation to an allowed state, while the outer electron remains as 'spectator', is manifested as a Seaton resonance. It is usually distinguishable because of its wider width. Seaton resonances are illustrated for excited states of Ar XIII (Nahar 2004) in Fig. 3. These resonances are seen only for valence electron excited states.
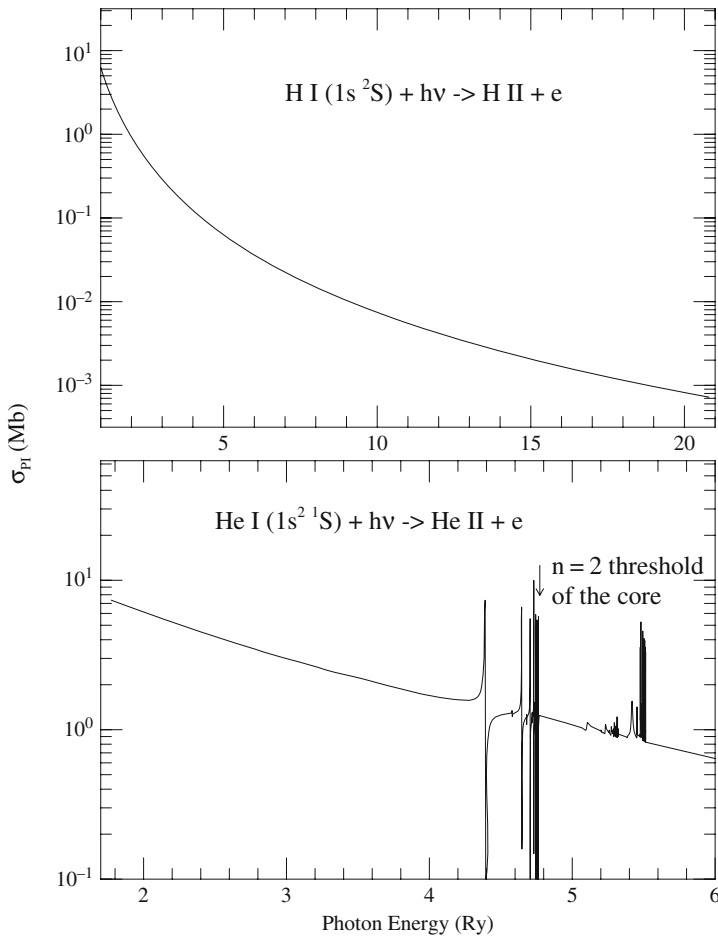
**Fig. 1.** Photoionization cross sections of ground levels of H and He. While $\sigma_{PI}$ for hydrogen is smoothly decaying, resonances exist for all atomic systems with more than one electron. They are formed due to doubly excited Rydberg states converging to core thresholds (e.g. n=2 for He).

$\sigma_{PI}$ of most of the complex atomic systems are obtained in LS coupling. However, relativistic BPRM is now implemented for fine structure levels of highly charged ions (e.g. Zhang et al. 2001). $\sigma_{PI}$ detailed with autoionizing resonances are available for many ions, as given in a partial list below, from the author and from http://vizier.u-strasbg.fr/topbase/topbase.htm:
C I, C II, C III, C IV, C V, C VI, N I, N II, N II, N IV, N V, N VI, N VI, N VII, O I, O II, O III, O IV, O V, O VI, O VII, O VIII, F IV, F VII, F VIII, F IX, Ne V, Ne VIII, Ne IX, N X, Na VI, Na IX, Na X, Na XI, Mg VII, Mg X, Mg XI, Mg XII, Al VIII, Al XI, Al XII, Al XIIL, Si I, Si II, Si IX, Si XII, Si XIII, Si XIV, S II, S III, S XI, S XIV, S XV, S XVI, Ar V, Ar XIII, Ar XVI, Ar XVII,
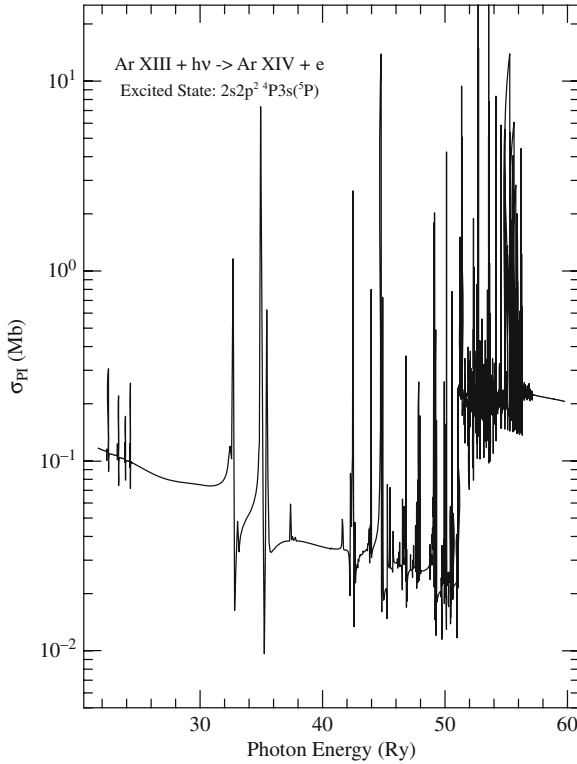
**Fig. 2.** Photoionization cross sections of the excited $2s2p^2\ ^4P3s(^5P)$ state of carbon-like Ar XIII illustrating resonant structures of a complex ion and effect on the enhancement of the background (Nahar 2004). The resonances arise due to Rydberg series of autoionizing states belonging to the core.

Ar XVIII, Ca VII, Ca XV, Ca XVIII, Ca XIX, Ca XX, Ti XX, Ti XXI, Ti XXII, Cr XXII, Cr XXIII, Cr XXIV, Fe I, Fe II, Fe III, Fe IV, Fe V, Fe XIII, Fe XVII, Fe XXI, Fe XXIV, Fe XXV, Fe XXVI, Ni II, Ni XXVI, Ni XXVII, Ni XXVIII.

# 4 Electron-Ion Recombination - Total and Level-specific Recombination Rate Coefficients

A typical behavior of the total recombination rate coefficient ($\alpha_R$) is: starts high at low temperature due to dominance by RR, falls with temperature and then rises again at high temperature due to dominance of DR forming a DR 'bump', followed by monotonic decay at very high temperature. An example is shown by the solid curve in Fig. 4 for $\alpha_R(T)$ of Fe XXIV (Nahar et al. 2001).
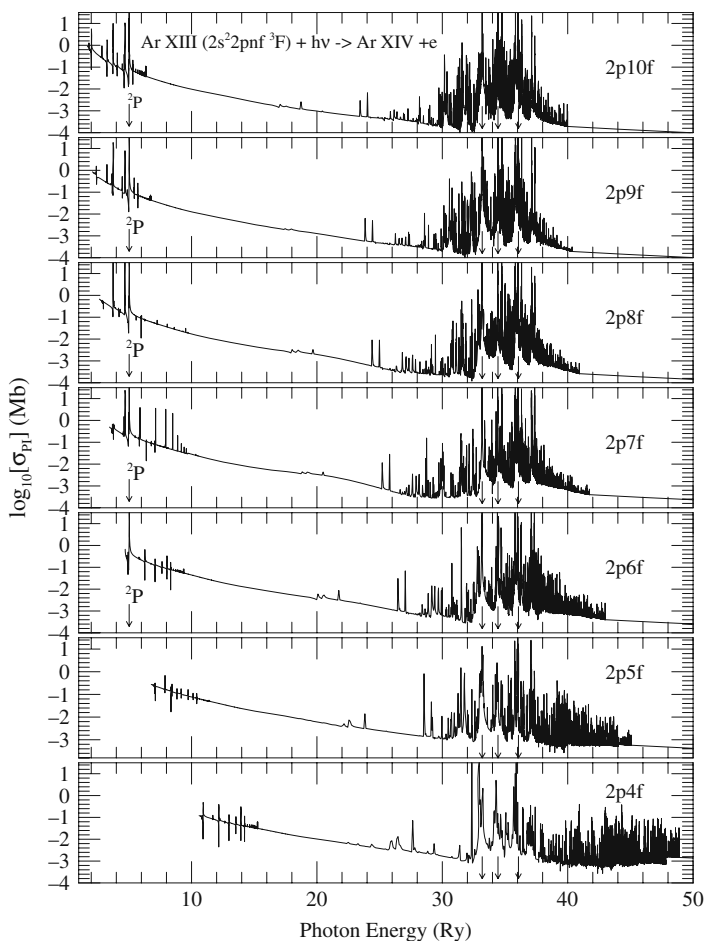
**Fig. 3.** Seaton resonances (at arrow positions) in photoionization cross sections of excited $2pnf\,^3F$ states, where 4f $\leq nf \leq$ 10f, of Ar XIII (Nahar 2004). These resonances show the non-hydrogenic behavior of excited states of an ion.

The typical feature changes with complex ions by forming multiple DR 'bumps'. Their locations depend on the resonance positions in photoionization. An example of two DR 'bumps' can be seen in $\alpha_R(T)$ of Fe II (Nahar 1997) in Fig. 5. The reasons for large differences are simpler central and hydrogenic approximations for RR rates (Arnaud & Raymond 1992), and inaccurate A-values and omission of autoionization to various states in the IRA approximation for DR rates (Woods et al. 1981).

One important advantage of the unified method is obtaining state-specific recombination rate coefficients $\alpha_R(nLS)$, including both RR and DR, for many bound levels. Figure 6 shows such rates for Fe XXI (Nahar 2007b). These rates are needed for the cascade matrix and determination of level
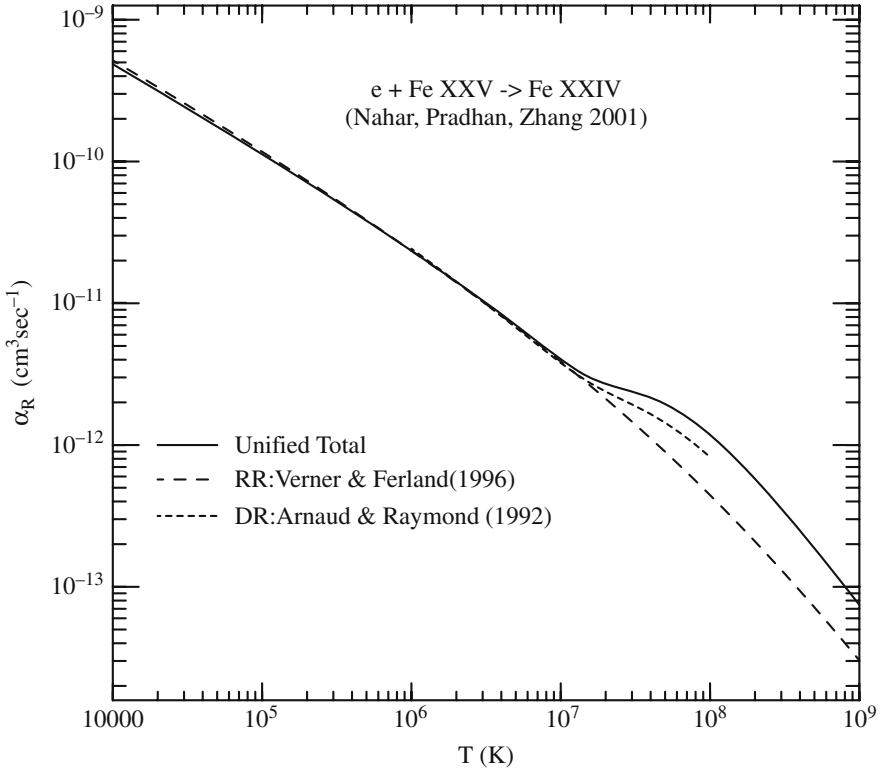
**Fig. 4.** Total recombination rate coefficients for (e+Fe XXV → Fe XXIV) from unified method (Nahar et al. 2001) are compared with RR rates (Verner & Ferland 1996) and DR rates (Arnaud & Raymond 1992).

populations. These rates as well as total $\alpha_R$ for many ions, as listed for photoionization above, are available from the author.

## 5 Plasma Opacity from the Opacity Project

Latest monochromatic opacities are available through OPserver at the website: http://opacities.osc.edu. OPserver provides interactive online-computations of opacities and radiative accelerations (Mendoza et al. 2007). Data available are Rosseland mean opacities (RMOs) and radiative accelerations (RAs) that can be used for any arbitrary chemical mixtures. The opacities are computed online directly from the OP monochromatic opacities. The mixture is specified by the hydrogen (X) and metal (Z) mass-fractions (X+Y+Z=1) and its metal fractional composition. The OP opacities were refined in December 2004 to include inner-shell contributions. The OPserver software were upgraded in June 2006 to enable local installations and library linking.
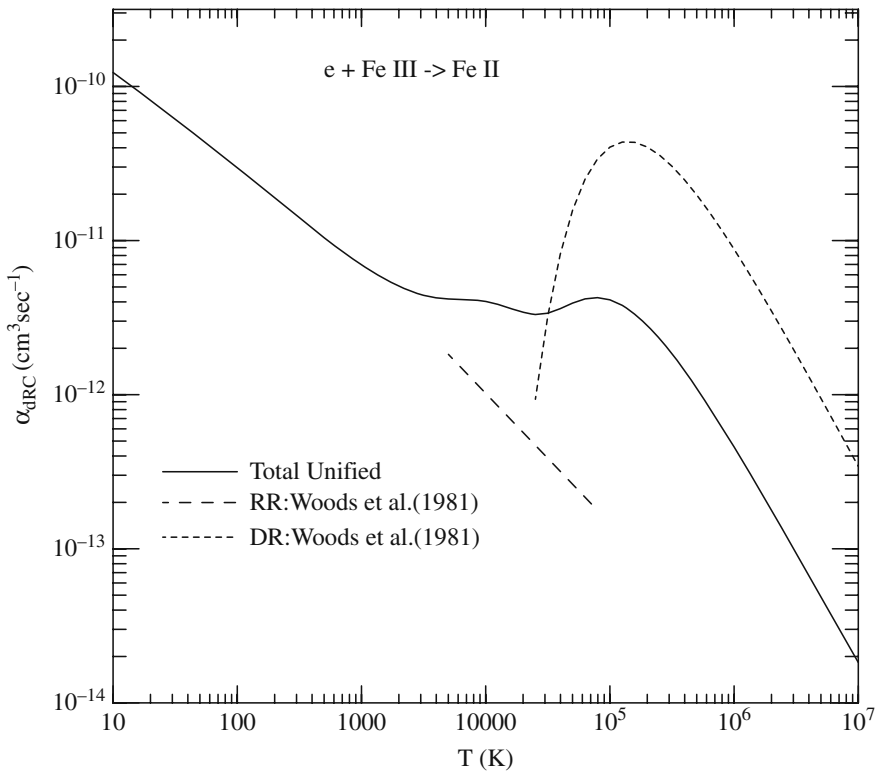
**Fig. 5.** Total unified recombination rate coefficients of Fe II showing multiple DR bumps (Nahar 1997). They differ from RR rates (Arnaud & Raymond 1992) and DR rates (Woods et al. 1981).

The complete $OPCD\_3.0$ package (data, codes and instructions) to compute locally RMOs and RAs and to install the OPserver can also be downloaded from the OP home page. Atomic data from the Opacity Project and Iron Project are accessible from this website.

# References

Arnaud, M., & Raymond, J. 1992, ApJ, 398, 394

*Atomic data from the Iron Project* series. 1993-Astron. Astrophys.; data files available at CDS.

Bell, R. H., & Seaton, M. J. 1985, J. Phys. B 18, 1589

Hummer D. G., Berrington K. A., Eissner W., et al. 1993, A&A, 279, 298 (IP)

Mendoza, C., Seaton. M. J., et al. 2007, MNRAS 378, 1031

Nahar, S. N. 1997, Phys. Rev. A 55, 1980
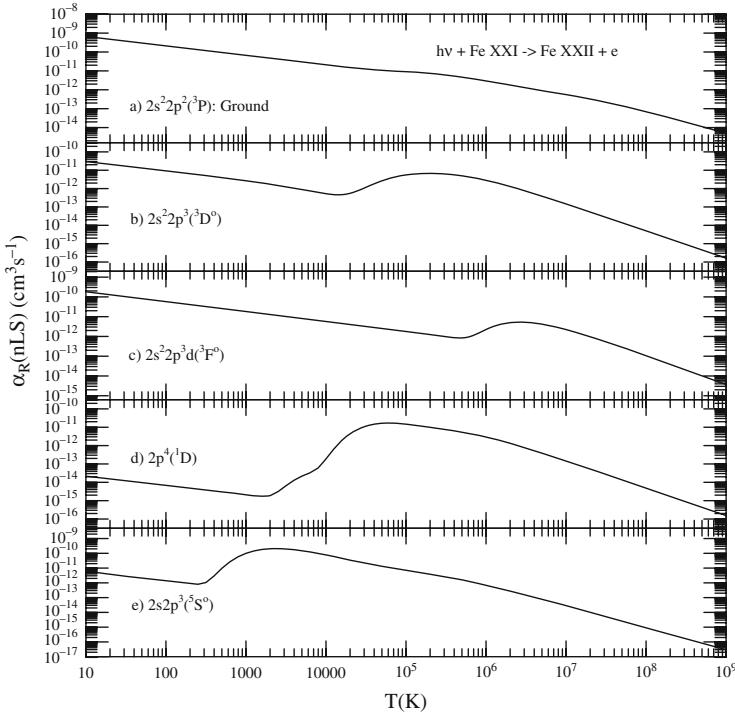
Nahar, S. N. 2004, ApJS, 156, 93

**Fig. 6.** State-specific recombination rate coefficients, including RR and DR, of Fe XXI (Nahar 2007b).

Nahar, S. N. 2007a (He cross sections are from R-matrix, unpublished)

Nahar, S. N. 2007b (to be submitted)

Nahar S. N., Eissner, W., Chen, G.X., & Pradhan, A.K. 2003, A&A, 408, 789

Nahar S. N., Eissner, W., Pradhan, A.K., & Sur, C. 2007, in preparation

Nahar, S. N., & Pradhan, A.K. 1992, Phys. Rev. Lett. 68, 1488

Nahar, S.N., & Pradhan, A.K. 1993, J. Phys. B 26, 1109

Nahar, S.N., & Pradhan, A.K. 1994, Phys. Rev. A 49, 1816

Nahar, S.N., & Pradhan, A.K. 2000, Phys. Scr. 61, 675

Nahar, S. N., Pradhan, A.K. & Zhang, H.L. 2001, ApJS 133, 255

Seaton, M. J., 1987, J. Phys. B, 20, 6363

*The Opacity Project vols 1 & 2*, compiled by the Opacity Project Team: Institute of Physics, London UK 1995 and 1996 — (OP)

Verner, D. A., & Ferland G. 1996, ApJS, 103, 467

Woods, D. T., Shull, J. M., & Sarazin, C. L. 1981, ApJ, 249, 399

Yu, Y., & Seaton, M. J. 1987, J. Phys. B, 20, 6409

Zhang, H. L., Nahar, S. N., & Pradhan, A. K. 1999, J. Phys. B, 32. 1459

Zhang, H. L., Nahar, S. N., & Pradhan, A. K. 2001, Phys. Rev. A, 64, 032719